The Vertical Structure and Development of the ENSO Anomaly Mode during 1979–1989*

BIN WANG

Department of Meteorology, School of Ocean and Earth Science and Technology, University of Hawaii, Honolulu, Hawaii

(Manuscript received 18 June 1991, in final form 30 August 1991)

ABSTRACT

The latest two Pacific basinwide warm episodes (1982–83 and 1986–87) exhibit some common features in their development and vertical structure. These features are examined by multivariate empirical orthogonal function analysis of the interannual variability of the ocean–atmosphere system along equatorial Indian and Pacific oceans.

The updraft and downdraft branches of the anomalous Walker circulation originate over the western Pacific and the eastern Indian Ocean, respectively. The early development of basinwide warming is characterized by the strengthening of a cross-equatorial low-level southerly component over the eastern Pacific and the enhancement of convection and boundary-layer westerlies over the western Pacific.

The structure of the ENSO anomaly mode changes from the cold to the warm phase of the Southern Oscillation. This is attributed to its eastward migration and the intrinsic longitudinal dependence of the vertical structure. The latter results from the east–west contrast of the air–sea interaction processes. Over Indonesia and the western Pacific, the land–sea thermal contrast and high SST maintain a semipermanent convective action center, whose intensity is sensitively modulated by small SST fluctuation. Since moist static ability is small, the surface pressure responds sensitively to the heating, so that the anomalous low pressure and associated zonal wind convergence in the boundary layer are in phase with the enhanced convection. In contrast, over the central-eastern Pacific, large SST gradient–induced pressure gradient force drives boundary-layer flows whose beta convergence determines atmospheric heating, while the feedback of the free atmosphere to boundary-layer flows is weak due to large static stability. The enhanced convection is thus nearly in phase with anomalous boundary-layer westerlies, positive zonal SST gradient, and negative zonal surface pressure gradient.

It is possible that an individual ENSO event may result from different combinations of various sets of coupled processes, especially with regard to those that work in the eastern Pacific cold tongue and those in the western Pacific warm pool.

1. Introduction

The El Niño–Southern Oscillation (ENSO) is a dominant mode of the interannual variability of the coupled ocean and atmosphere climate system. Based on the analysis of six warm episodes that occurred between 1950 and 1979, Rasmusson and Carpenter (1982, hereafter denoted as RC) found that the phases of the warm events appear to be closely related to those of the annual variation. A composite El Niño in seasonal sequence was thus described. Their major findings were recently confirmed and extended by composite studies of Wright et al. (1988) and Deser (1990).

The RC composites show an early weak warming in the western Pacific, but the major warming first appears along the South American coast and subsequently is found farther west along the equator. However, during the exceptionally strong 1982–83 warm episode, the warming in the central Pacific leads that in the eastern Pacific (Gill and Rasmusson 1983; Rasmusson and Wallace 1983). The 1986–87 warm episode bears similarities, in many aspects, to the 1982–83 event. The common features of the latest two warm episodes will be described in this paper.

Figure 1a indicates that the interannual variability of outgoing longwave radiation (OLR) exhibits maxima in the central equatorial Pacific and east of Borneo around 130°E. There is a distinguished equatorial band between 7°N and 5°S from 120°E to 80°W where the interannual variance exceeds 1.58 times of the annual variance (Fig. 1b). The present analysis will focus on this core region of ocean–atmosphere interaction, where SST, convection, and surface zonal wind anomalies all attain maxima and the ocean responds to the wind forcing most sensitively.

Although the major warming area during an El Niño is confined to the equatorial eastern and central Pacific, the ENSO variability in the equatorial western Pacific is remarkably large compared with the annual variability in situ. The eastward expansion of the region of high SST from the western Pacific warm pool is a common feature in the development of all El Niño episodes (Fu et al. 1986). The atmospheric variability

* Contribution Number 2764 from the School of Ocean and Earth Science and Technology, University of Hawaii.

Corresponding author address: Dr. Bin Wang, University of Hawaii, School of Ocean & Earth Science & Technology, Department of Meteorology, 2525 Correa Rd—HIG 331, Honolulu, HI 96822.

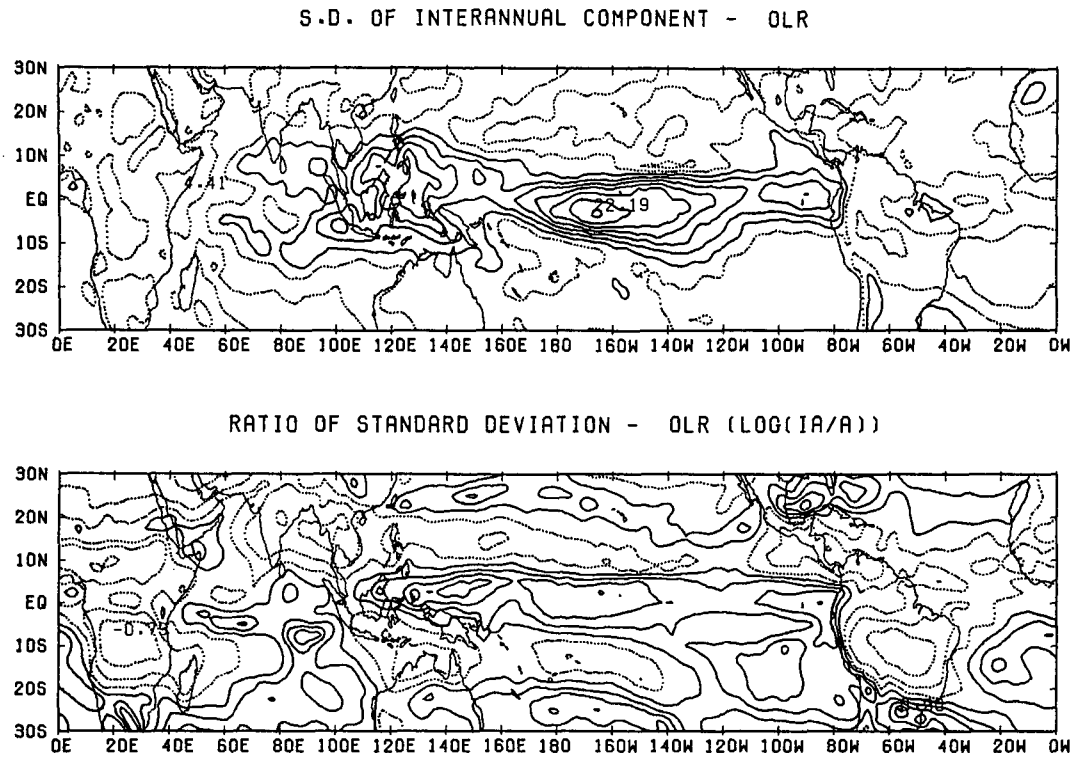

FIG. 1. Contour plot of (top) standard deviation of the interannual component of OLR (contour interval is 2 W m^{-2} and the solid contours start from 10 W m^{-2}), and (bottom) logarithmic ratio of the standard deviation of interannual vs annual component. Contour interval is 0.2 and solid (dotted) lines denote positive and zero (negative) contours. The logarithmic ratio 0.2 means 1.58 times. The data cover the interval from 1980 to 1987. The definition of interannual and annual component is as in the text (section 2a).

associated with Pacific basinwide SST changes is even far more reaching in areal extent. The collapse of the trade winds during El Niño (Wyrtki 1975) tends to be coupled with the eastward progression of the monsoons from the Indian Ocean into the central Pacific (Barnett 1984a,b). The eastward-propagating signals in the equatorial band were also documented by Yasunari (1985) using 200-mb near-equator wind data and by Gutzler and Harrison (1987) using multilevel rawinsonde data from six near-equator stations. The close relationship between the Indian summer monsoon and the interannual variation of the tropical Pacific suggests that the Asian monsoon may have an active role in the interannual variability of the coupled atmosphere–ocean system (Meehl 1987; Yasunari 1990; Rasmusson et al. 1990). In view of this, the present study investigated the behavior of the coupled mode over both the equatorial Pacific and Indian oceans.

In the last decade, a large number of simple and intermediate coupled ocean–atmosphere models have been developed to elucidate the mechanisms responsible for the ENSO variabilities of the coupled system (e.g., Philander et al. 1984; Hirst 1986; Zebiak and Cane 1987; Battisti 1988; Neelin 1990). Theoretical understanding of dynamic behavior of the ENSO mode requires detailed knowledge of the evolution and structure of the coupled mode in both media. Despite the unprecedented effort that has been put into description of the phenomenon, the vertical structure and development characteristics have not been well documented from coherent variations of SST and atmospheric variables. The present study examines the development and vertical structure of the coupled anomaly mode during the 1980s. Particular attention is paid to the common features of the recent two warm events and the differences in the behavior of the coupled mode between warm and cold phases of the Southern Oscillation (SO). Evidence will be presented to show that the vertical structure of the ENSO anomaly mode has an intrinsic geographical dependence. This is caused essentially by different sets of coupling mechanisms operating, respectively, in the eastern Pacific (cold tongue–open ocean processes) and the western Pacific (warm pool–large tropical island processes).

The data to be analyzed are discussed in section 2 along with a brief introduction to the procedure of multivariate empirical orthogonal function (MV-EOF) analysis. This method enables us to reveal coherent variations among oceanic and atmospheric variables and define an ENSO anomaly mode. The development and vertical structure of the ENSO anomaly mode are then described in sections 3 and 4, respectively. In sec-

tion 5 an explanation of the temporal and zonal variations of the vertical structure of the ENSO anomaly mode is offered. Section 6 contains conclusions and discussions.

2. Data processing and the method of multivariate EOF analysis

a. *Monthly mean data and the interannual component*

The monthly mean data include seven atmospheric and oceanic variables: SST, sea level pressure (p_s), surface zonal (u_s) and meridional (v_s) winds, 850-mb and 200-mb zonal wind (u_{850} and u_{200}), and OLR. All datasets cover the 11-year interval from January 1979 to December 1989 during which the latest two Pacific warm episodes occurred. The SST and surface pressure data have been extended to cover a longer period from January 1971 to December 1989.

The SST and the atmospheric surface variables are derived from individual ship reports of COADS (Comprehensive Ocean–Atmosphere Data Set) along the equatorial belt between 5°N and 5°S. The scarcity of ship-of-opportunity observations over the tropical oceans precludes high-resolution examination of the spatial and temporal variation. For the purpose of studying large-scale interannual variation, a time resolution of one month and spatial resolution of 10° longitude by 10° latitude square centered at the equator are adopted. The original ship reports were first sorted into 24 squares along the equator from 40°E to 80°W. Our analysis focuses on the equatorial strip. Duplicated and apparently unreasonable data were first discarded. Means (m) and standard deviations (s) for each variable at each square were then calculated. Individual values that fall outside the range ($m - ks$, $m + ks$) were removed, where k was taken as 3.5 for SST and sea level pressure, and 4.0 for surface wind components. This quality-control scanning was repeated twice. Figure 2 shows averaged observation numbers per month at each square. The poorest regions of observation are near the date line between 170°E and 170°W and in the eastern Pacific between 150°W and 110°W, where the monthly observation numbers are between 32 and 50. These numbers of observations are believed adequate to make representative monthly means.

The OLR data are derived from NOAA polar orbiter satellite observations. The 850- and 200-mb wind fields are extracted from objectively analyzed data prepared by the European Centre for Medium-Range Weather Forecasts (ECMWF). The OLR and 200- and 850-mb wind data have the same spatial and temporal resolution as those of the surface variables.

To focus on interannual variation, the monthly mean time series of each variable at each square is decomposed into three orthogonal low-frequency components using Fourier analysis: the interannual, annual, and intra-annual components. The interannual component includes variations with periods longer than 1 year; the annual component is defined as the sum of the two harmonics with periods of 1 year and 0.5 year, respectively; the intra-annual component describes variability on time scales from 4 months up to 1 year with the annual and semiannual harmonics excluded.

Table 1 presents the longitudinal dependence of relative variance of annual versus interannual components for each variables. The interannual components have the largest contribution to the total variances over the western and central Pacific (130°E–130°W) for all variables except v_s, whereas the annual components dominate over the Indian Ocean for all variables except OLR for which the intra-annual component has the largest contribution. Indonesia is a transition region in which the fractional annual variance decreases while interannual variance increases: most variables exhibit the largest fractional variance in annual variation except for surface pressure and 850-mb zonal wind, which display dominant interannual variations. In the eastern Pacific, both the fractional annual and interannual variance are large. Most variables are dominated by annual variation except for 850-mb zonal wind and OLR.

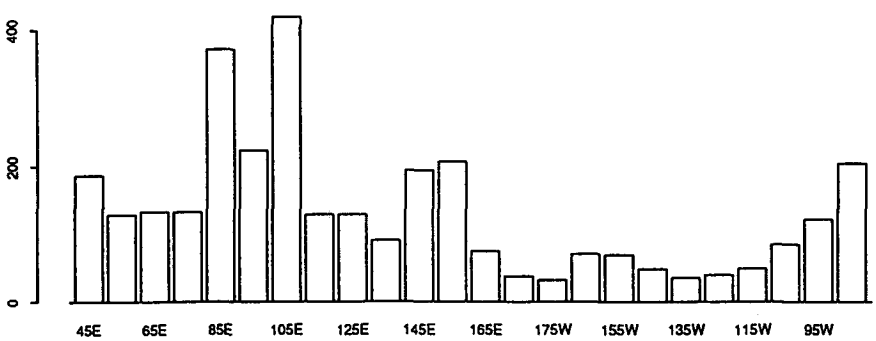

FIG. 2. Averaged observation numbers per month at each 10° square along the equator from 40°E to 80°W for the interval 1979–1989.

TABLE 1. Fractional (percent) variances along the equator; IA and A represent the interannual and annual component, respectively. Relative maxima are in italic.

	Variables													
	SST		u_s		u_{850}		OLR		u_{200}		p_s		v_s	
Longitude	A	IA	A	IA	A	IA	A	IA	A	IA	A	IA	A	IA
Indian Ocean (40°–100°E)	*73*	13	*70*	8	*46*	30	32	12	*53*	24	*43*	15	*92*	2
Indonesia (100°–130°E)	*66*	18	*41*	26	22	*36*	*40*	31	*42*	29	19	*40*	*94*	2
Western Pacific (130°E–180°)	18	*42*	17	*41*	27	*47*	15	*52*	31	*45*	21	*37*	*71*	11
Central Pacific (180°–130°W)	11	*71*	9	*50*	5	*77*	11	*76*	30	*54*	24	*27*	*52*	24
Eastern Pacific (130°–80°W)	*53*	37	*30*	21	7	*58*	16	*64*	*51*	24	*42*	32	*55*	19
Indian and Pacific (40°E–80°W)	*42*	37	*35*	29	23	*50*	22	*47*	*42*	35	*31*	29	*72*	12

In the rest of this paper all analyses were performed using the interannual components unless otherwise stated.

b. *The method of multivariate EOF analysis*

Conventional EOF, by making use of the property of spatial correlation, describes variations of a geophysical field with a relatively small number of functions and associated time coefficients. Geophysical fields are usually not only highly correlated in space but also significantly correlated with other fields. The multivariate EOF (MV-EOF) analysis extends conventional EOF by use of both spatial and intervariable coherence. It enables a more efficient compaction of multifield data. More important, it may extract dominant patterns in the spatial phase relationships among various fields of the derived empirical orthogonal functions. This often leads to physical insight into the interactive processes within a complex system such as the ocean–atmosphere climate system.

Consider simultaneous variations of I variables (fields). Assume we have a sample event of $Y = (y_{ijk})$ that consists of I variables ($i = 1, \cdots, I$) at J locations ($j = 1, \cdots, J$) sampled at K times ($k = 1, \cdots, K$). In order to analyze coherent variations of all I fields, normalized anomaly series for each field are formed first:

$$\tilde{y}_{ijk} = \frac{(y_{ijk} - \bar{y}_i)}{\sigma_i}, \quad i = 1, 2, \cdots, I$$

where $\bar{y}_i$ and σ_i are the mean and standard deviation of the ith field, respectively. The normalized anomaly series for each field has identical total variance JK.

The next step is to form a combined normalized anomaly data matrix

$$\mathbf{Z} = (z_{mk})$$

where $m = 1, 2, \cdots, IJ$, $z_{1k}, \cdots, z_{Jk}$ corresponds to y_{1jk}, ($j = 1, \cdots, J$), and $z_{J+1,k}, \cdots, z_{2J,k}$ corresponds to y_{2jk} ($j = 1, \cdots, J$), etc.

The subsequent analysis of event **Z** is identical to single variable EOF analyses. The derived empirical function has dimension IJ, which can then be decomposed to spatial patterns for I different fields in the same order as the data matrix was formed. In this way, the coherent structure among various fields is obtained along with a unified temporal evolution.

In principle, only when the variables under consideration are physically or statistically well correlated, the obtained principal eigenmodes contribute significantly to the total variance of all fields, so that the multivariate EOF yields meaningful results. It is important to realize that each field usually has uneven contribution to the variance carried by a combined EOF, say $E^{(n)}$. The variance carried by $E^{(n)}$, $V^{(n)}$ can be decomposed into I components, which correspond to the partial variance contributions from each field, $V_i^{(n)}$, $i = 1, 2, \cdots, I$. Since the total variance of each normalized field is equal to JK, the quantity

$$FV_i^{(n)} = \frac{V_i^{(n)}}{JK}, \quad i = 1, 2, \cdots, I$$

measures, on the one hand, the magnitude of partial variance contribution of the ith field to the variance carried by eigenfunction $E^{(n)}$, and, on the other hand, the fractional variance described by $E^{(n)}$ for the ith field. Analysis of fractional variance of each field helps to elucidate the nature of coupling among various fields.

3. The development characteristics of the ENSO anomaly mode

a. *Equatorial ENSO index*

Wright et al. (1988) noticed that the difference in surface pressure between Darwin, Australia, and the equatorial eastern Pacific is more intimately correlated with SSTs in the equatorial Pacific than is the conventional Southern Oscillation index based upon the pressure differences between Darwin and the subtropical southeast Pacific. To facilitate multivariate EOF anal-

ysis, in this subsection an equatorial ENSO index is defined in terms of EOF analysis of the SST and pressure field along the equator. The data used cover a period of 19 years, from January 1971 to December 1989.

The first EOF of the SST field accounts for 79% of the total interannual variance. The spatial structure along with the principal component, $C_1(t)$, shows that remarkable warming covers the entire eastern and central Pacific (80°W–160°E) with a maximum occurring around 125°W, about 2.5°C for the 1982–83 episode and 1.6°C for the 1986–87 episode (Fig. 3). The western Pacific from 120°E to 160°E exhibits a slight cooling during the warm episodes with a maximum cooling of 0.7°C for 1982–83 event and 0.4°C for the 1986–87 event. The central Indian Ocean tends to be in phase with the central and eastern Pacific, having weak warming. Since the E_1 mode dictates the interannual variation, its associated principal component may be used to define an index for the equatorial eastern-central Pacific warming.

The first EOF of surface pressure field accounts for 62% of total interannual variance. Its structure is characterized by a high at the western Pacific (135°E) and a low at the far eastern equatorial Pacific (95°W) (Fig. 3a). The associated principal component (Fig. 3b) provides an equatorial index for the SO. A previous study (Deser 1990) found that during the warm episode a low-pressure anomaly center was at the east end of the equatorial Pacific, which was separated from the Southern Hemisphere anomaly center. This adds confidence to the present definition of the equatorial SO index.

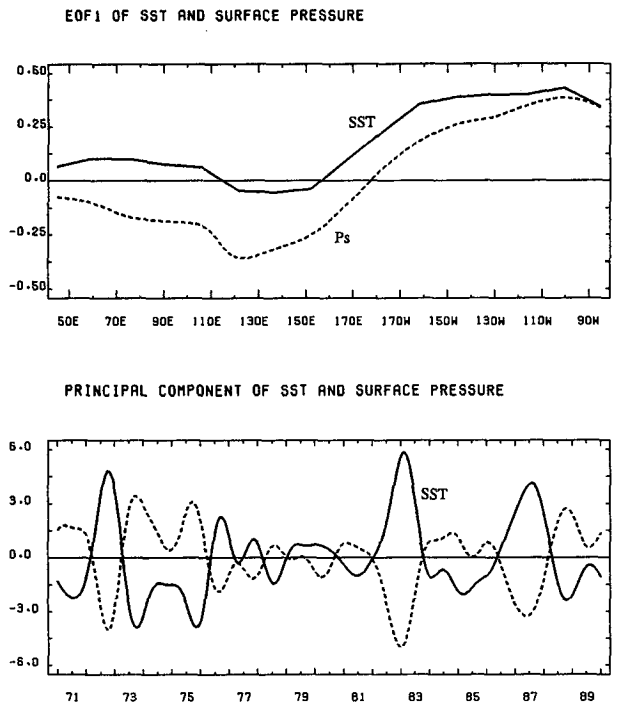

FIG. 3. (a) The first empirical orthogonal functions and (b) corresponding principal components of the SST and surface pressure over the equatorial Indian and Pacific oceans. Year labels reflect month of July.

Since the first principal component of the pressure field is almost exactly out of phase with that of the SST field (Fig. 3b), the principal component of the first EOF of SST field is used as an equatorial index for both Pacific basinwide warming and SO and is referred to as equatorial ENSO index. Positive (negative) values of the index indicate eastern-central Pacific warming (cooling) and negative (positive) swing of the SO.

We note that the peak warming of 1972 and 1976 ENSO events occurs in boreal fall (October and September), whereas the peak warming of the 1982–83 and 1986–87 events occurs in February and June, respectively (Fig. 3b). The seasonal warming occurs off the coast of South America and far eastern equatorial Pacific in boreal spring and propagates westward (Horel 1982). Rasmusson and Carpenter (1982) noticed this as a possible connection to the evolution of their composite ENSO events that begin in late boreal spring. The onset of the 1982–83 ENSO event was June 1982, corresponding to the RC composite, although the anomalies moved eastward. The 1986–87 event, however, has an odd seasonal onset in November. This indicates that the timing of the latest two Pacific basinwide warming is quite different from that of the two events in the 1970s. A composite technique in seasonal sequence is inadequate for the recent two events.

b. Multivariate EOF analysis

An MV-EOF analysis of the combined seven atmospheric and oceanic fields has been performed. The first EOF, E_1, exhibits intense warming in the eastern Pacific (maximum is at 125°W), slight cooling in the western Pacific, and weak warming in the Indian Ocean. In association with the SST pattern, surface pressure falls at the east end of the equatorial Pacific and rises in the western Pacific; enhanced convection and associated surface westerly and 200-mb easterly anomalies occur in the Pacific around 160°W (Fig. 4a). The corresponding temporal variation, $C_1(t)$, is best linearly correlated simultaneously with the equatorial ENSO index. The correlation coefficient is 0.96 (Table 2). Thus, the spatial pattern of E_1 represents the extreme phases of ENSO. The principal component associated with E_1, $C_1(t)$, reaches maximum during the mature phases of the latest two Pacific basinwide warm episodes and reaches a prominent minimum during the mature phase of the 1989 cold episode.

The second EOF, E_2, depicts a central Pacific warming pattern: sea surface warms and pressure falls in the central Pacific (160°W) and enhanced convection,

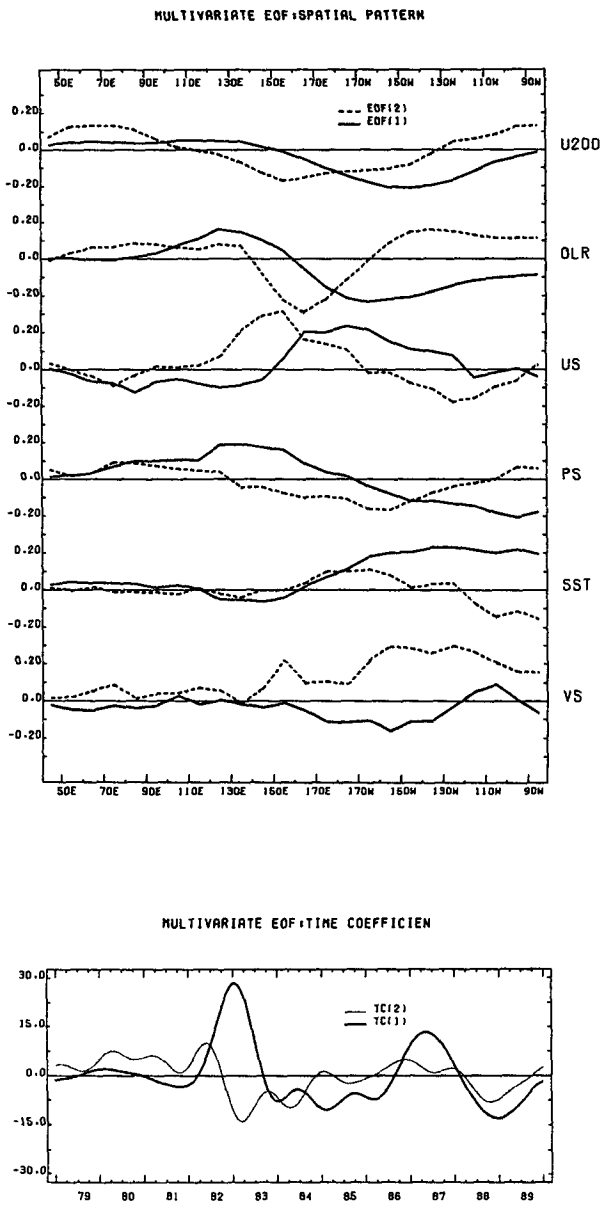

FIG. 4. (top) The first and second empirical orthogonal functions E_1 and E_2 and (bottom) the corresponding principal components, $C_1(t)$ and $C_2(t)$, derived from the multivariate EOF analysis of the interannual components for seven atmospheric and oceanic variables. Plotted here are only six variables.

surface westerly, and 200-mb easterly anomalies appear in the western-central Pacific centered around 160°E (Fig. 4a). Its principal component, $C_2(t)$, leads the equatorial ENSO index by 8–10 months with a correlation coefficient of 0.50 (the correlation coefficient is well above the 99% confidence level) (Table 2), suggesting that the spatial pattern of E_2 may be viewed as representative of the early warming (cooling) phase of the warm (cold) episodes. Since the amplitude of E_1 is comparable to that of E_2, while the amplitude of $C_1(t)$ is larger than that of $C_2(t)$, the development of both the warm and cold events is obvious.

In what follows, the sum of the first two EOFs, $C_1E_1 + C_2E_2$, will be referred to as the ENSO anomaly mode. For the combined seven fields as a coupled system, E_1 and E_2 contribute to the total interannual variance by 50% and 17%, respectively; thus, the ENSO anomaly mode accounts for 67% of the total interannual variances for the seven fields. Each field, however, has a different contribution to the variance carried by the combined E_1 and E_2 modes. The fractional variances described by E_1 and E_2 for each individual field are listed in Table 3, which discloses several interesting features.

First, the ENSO anomaly mode has a large projection (69%–81%) on the interannual variations of the OLR, SST, u_{850}, and u_s, fields, indicating the presence of an intimate coupling among these four fields. On the other hand, a relatively small projection (52%–55%) of the ENSO mode on the v_s and u_{200} fields suggests that these two fields contain more non-ENSO variabilities.

Second, the E_1 mode accounts for 57% to 69% of the total variance of the SST, OLR, u_{850}, and p_s fields, and a much smaller fractional variance for u_{200} and v_s fields. This means that during the peak phase of the warm episode the changes in SST, u_{850}, OLR, and p_s fields are relatively more significant than the changes in v_s and u_{200} fields. The E_2 mode, or the early warming, however, displays relatively large changes in surface cross-equatorial flow (v_s), significant changes in convection (OLR), and surface and 850-mb zonal winds, but insignificant changes in the SST and surface pressure fields. This reveals that the early warming is hardly detectable from changes in SST and p_s fields but more evident from changes of surface meridional and zonal wind and convection fields.

TABLE 2. Lag correlation coefficients (r) between the equatorial ENSO index and the first two principal components, $C_1(t)$ and $C_2(t)$, of the multivariate EOF analysis. Positive lag means $C_1(t)$ or $C_2(t)$ lags ENSO index. $|r| = .24$ corresponds to 99% confidence level.

	Lag (month)										
	−10	−8	−6	−4	−2	0	2	4	6	8	10
$C_1(t)$	.10	.34	.58	.78	.92	.96	.89	.73	.51	.27	.05
$C_2(t)$	.50	.49	.41	.27	.12	−.01	−.11	−.18	−.25	−.34	−.43

TABLE 3. Fractional variances for each field carried by E_1 and E_2 of MV-EOF analysis.

	SST	p_s	u_s	u_{850}	OLR	u_{200}	v_s	Mean
E_1	.69	.57	.48	.59	.61	.41	.18	.50
E_2	.06	.08	.21	.18	.20	.14	.34	.17
$E_1 + E_2$	.75	.65	.69	.77	.81	.55	.52	.67

The results in Table 3 along with the pattern of E_2 in Fig. 4a reveal that the enhancement of the cross-equatorial southeast trade winds in the eastern Pacific (150°–100°W), and the enhancement of convection around 165°E and surface westerlies in the western-central Pacific (130°E–170°W) are two characteristic signals of the early ENSO development. The first signal has not received enough attention, albeit the second has been repeatedly emphasized in the literature. The strong cross-equatorial flow from the south in the eastern Pacific about 8 months before the major warm events can also be found in the composite ENSO of Rasmusson and Carpenter (1982) and Rasmusson et al. (1986). These early stage development features are common for both 1982–83 and 1986–87 warm episodes. However, caution must be exercised with these signals, because the E_2 mode primarily characterizes a weak central Pacific warming, which may be just an indication of local warming limited in the west-central Pacific region without further developing a major warming in the eastern Pacific (such as the cases in early 1980 and 1981). A key problem for prediction of this type of ENSO is to find out under what conditions the development of weak mid-Pacific warming and moderate convection and surface westerly anomalies over the western-central Pacific will further intensify, resulting in a major eastern Pacific warm episode.

Figure 5 shows a longitude–time diagram of the ENSO anomaly mode reconstructed using the first two MV-EOFs, which reveals where the anomalous Walker cell originates during ENSO warm episodes. There are two centers of large ENSO variability for convection. One is located east of Borneo around 125°E, and the other is in the central Pacific around 160°W (Fig. 5e, also Fig. 1). These are the preferred locations for the updraft and downdraft branches of the anomalous Walker circulation. We note that, during the cold phase, the eastern anomalous Walker cell to the east of the updraft region is stronger than the western cell, extending from the maritime continent to equatorial Africa (Figs. 5c–f). In the transition from the cold to warm phase, the eastern anomalous Walker cell weakens, while the western cell magnifies with a pronounced downdraft strengthening over the Indian Ocean. This western Walker cell then moves eastward and becomes a dominant cell at the peak warm phase. Therefore, the anomalous Walker circulation associated with the Pacific basinwide warming seems to originate and develop in the vicinity of the maritime continent. The updraft branch of the anomalous Walker circulation seems to intensify in the western Pacific near the date line for both the recent warm episodes. The development mechanisms over the warm pool region probably differ from those in the cold eastern-central Pacific and deserve further theoretical studies.

4. The vertical structure of the ENSO mode

a. Evolution of the structure from cold to warm phase

During the peak cold phase of Southern Oscillation (e.g., January 1989 and February 1985), SST is slightly higher than normal in the western Pacific warm pool around 140°E (Fig. 6). The anomalous low pressure is nearly below the enhanced convection at 125°E. The maximum 850-mb and surface westerly anomalies are about 40° to the west of the enhanced convection center, while the boundary-layer easterly anomalies are located east of the convection center over the central Pacific. This structure represents a weak intensification of a normal Walker cell.

About one-half year before commencement of the warm episodes (October 1981 and April 1986), the overall structure (Fig. 7a) is essentially the same as that normally found in the cold phase except for the smaller amplitude. Enhanced southeasterly trades develop in the central Pacific around 155°W (not shown).

At the time of onset of the warm episodes (June 1982 and November 1986), the vertical structure of the ENSO anomaly noticeably changes (Fig. 7b). The enhanced convection migrates to the date line. The positive SST anomaly displays double peaks with a minor peak situated at 20°–30° and a major peak about 50° ahead (east) of the enhanced convection. The 850-mb and surface westerly anomalies become nearly in phase with the enhanced convection at this stage. Another pronounced change is that the surface low pressure previously located near the maritime continent now is replaced by an anomalous high pressure, whereas the original low pressure anomaly swiftly moves to 145°W, about 30° east of the convection anomaly. The enhanced southerly wind remains about 70° east of the enhanced convection. There is a rapid transition between prewarm and initial warm phase during which the surface pressure and zonal wind fields

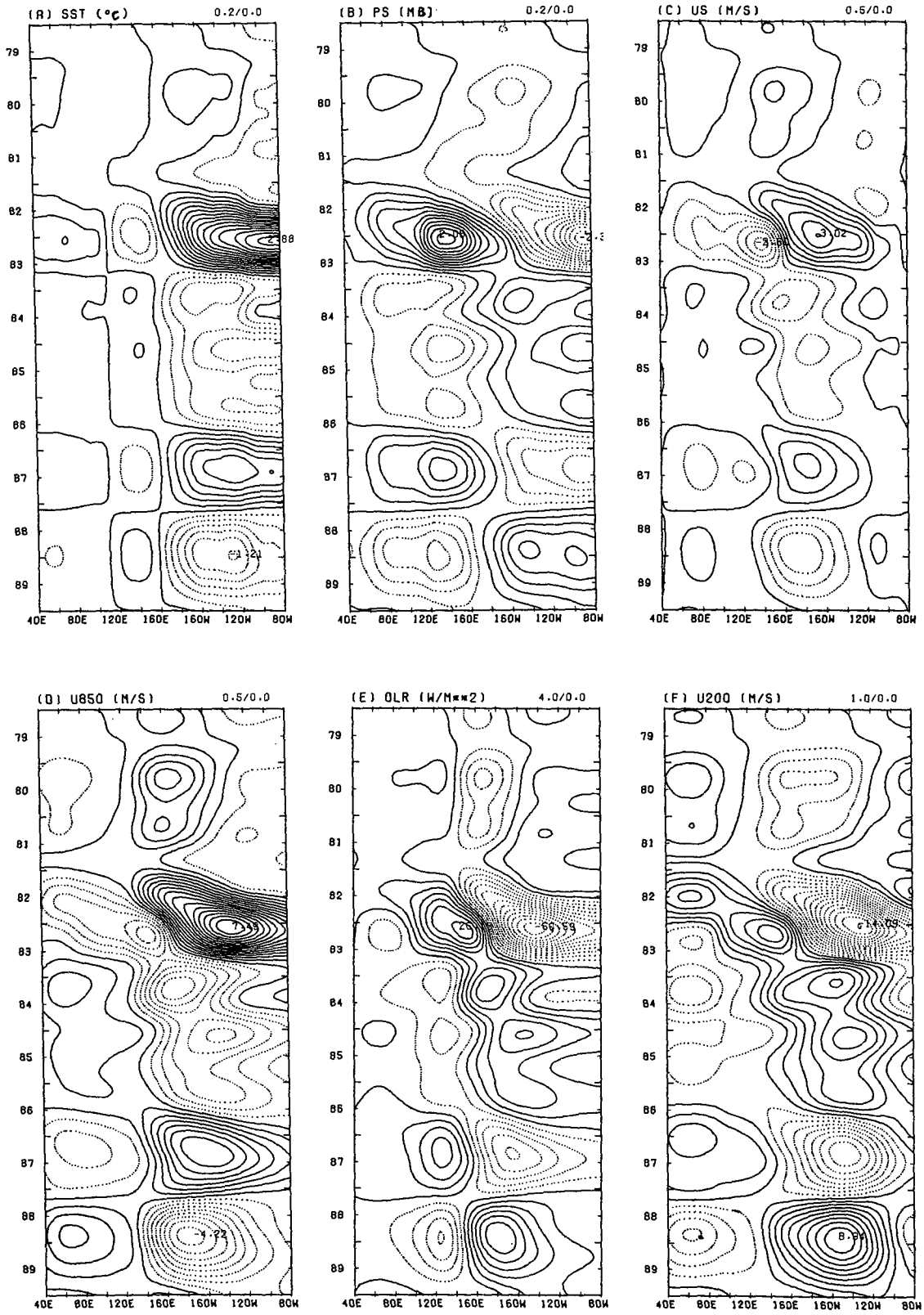

FIG. 5. Longitude–time diagram of the ENSO mode defined by the sum of the first two multivariate EOFs $(C_1(t)E_1 + C_2(t)E_2)$ for SST, p_s, u_s, u_{850}, OLR, and u_{200}. The units for u_s, u_{850}, and u_{200} are meters per second, the units for SST, OLR, and p_s are degrees Celsius, watts per meter squared, and millibars, respectively. Year labels reflect month of July.

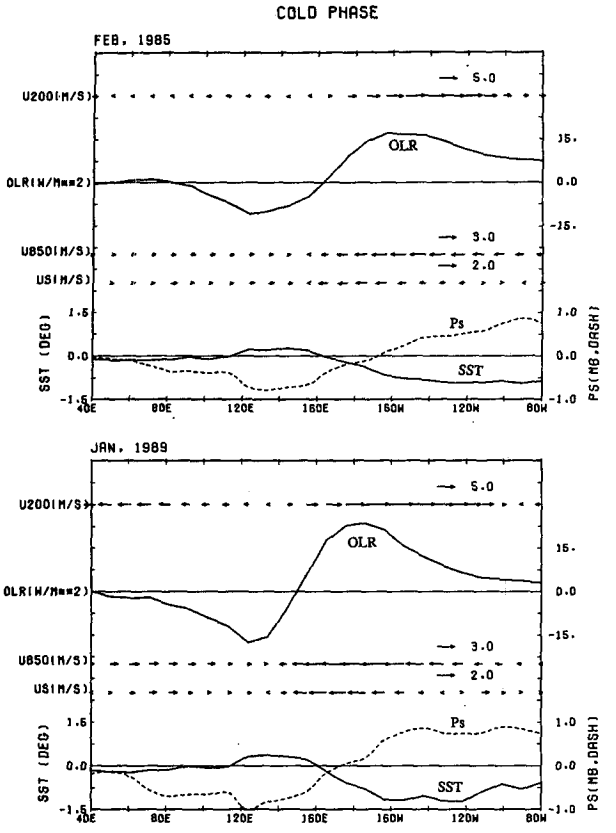

FIG. 6. Vertical structure of the ENSO anomaly mode in the cold phase of the Southern Oscillation (February 1985 and January 1989).

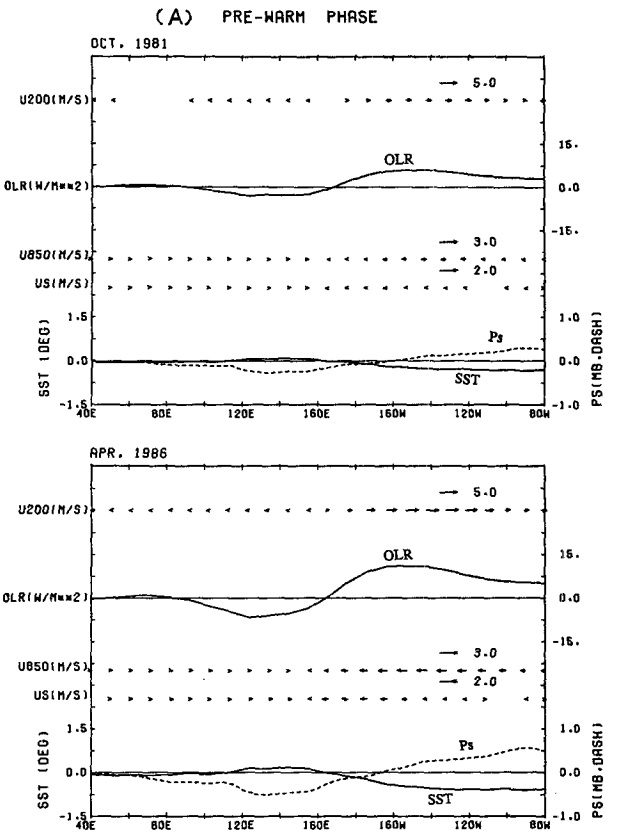

FIG. 7. Vertical structure of the ENSO anomaly mode in the equatorial zonal plane at three different phases for both 1982–83 and 1986–87 warm episodes: (a) prewarm, (b) initial warm, and (c) peak warm.

undergo rapid eastward shift so that the coupling between the SST and u_s (and p_s) fields becomes more intimate.

In the peak warm phase (January 1983 and May 1987) (Fig. 7c) and decay phase (July 1982–83 and October 1987) (not shown), the phase relationships among convection, SST, and surface and 850-mb zonal wind anomalies do not exhibit significant changes; the structure of the ENSO anomaly is, therefore, similar to that of the onset phase except the spatial phase lag between the surface low and convection anomalies becomes larger.

Previous studies (Murakami and Sumathipala 1988) found that during the 1976–77 ENSO event, the highest SST anomaly appears to occur three months prior to the lowest OLR anomaly on the interannual time scales. This temporal phase difference is equivalent to a spatial phase difference of about 24° longitude with positive SST anomaly leading negative OLR anomaly if the mean speed is about 8° longitude per month. Thus, the spatial phase difference between OLR and SST found in Fig. 7 is consistent with Murakami and Sumathipala's result. Deser (1990) observed that the convection anomaly is characterized by anomalous low-level wind convergence, but the meridional winds make dominant contribution to the low-level convergence. In Figs. 7b and 7c the boundary-layer zonal wind anomalies are nearly in phase with enhanced convection, implying that the convergence due to zonal wind component $\partial u/\partial x$ has little contribution to total boundary-layer convergence; thus, the meridional wind-induced convergence $\partial v/\partial y$ must be the principal part of the total boundary-layer convergence. Therefore, the phase relationship between convection and boundary-layer zonal wind anomalies derived for the ENSO anomaly mode is consistent with Deser's composite ENSO although the datasets cover different warm episodes.

b. Longitudinal variation of the vertical structure

Some features of the vertical structure of the ENSO anomaly mode stay nearly the same across the entire equatorial Pacific and Indian oceans and for both warm and cold phases of the SO. For instance, Table 4 shows the linear correlation coefficients calculated for ENSO

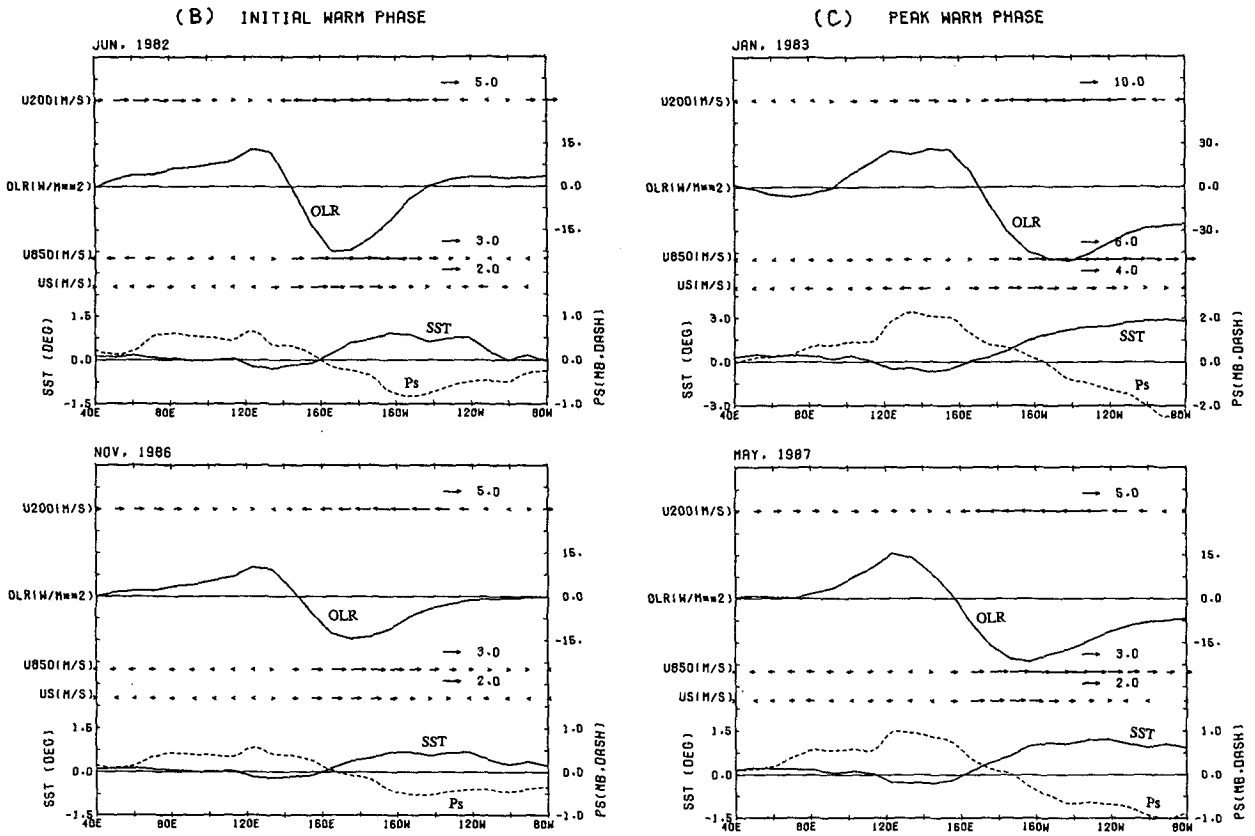

FIG. 7. (*Continued*) Notice that different scales are used for the peak phase of 1982–83 episode (the upper panel of Fig. 7c).

anomaly mode and interannual component, respectively; the sample size was 824. All values exceed the 99% confidence level. The zonal wind at 850 mb is approximately in phase with surface zonal wind and out of phase with 200-mb zonal wind. This indicates that the ENSO mode, to the lowest order, has the structure of the gravest baroclinic mode in the free atmosphere and barotropic structure in the boundary layer. The magnitude of zonal winds, however, increases significantly with altitude in both the free atmosphere and boundary layer. Based on linear regression equations, the magnitude of the 200-mb zonal wind is about two and one-half times that at 850 mb, and the magnitude at the surface is about one-half that at 850 mb. This suggests that higher-order baroclinic modes must be considered if the asymmetric vertical structure in the free atmosphere is to be explained. The increase of zonal wind with height in the boundary layer results from the boundary-layer frictional effect and agrees well with Harrison and Gutzler's (1986) estimation for seasonal means.

In contrast to the foregoing longitude-independent features, the spatial phase relationships between convection (negative OLR) and SST, convection and surface pressure, and convection and surface zonal wind have remarkable longitudinal variations.

The spatial phase difference between convection and SST anomalies varies with longitude (Figs. 5, 6, and 7c). Over the Pacific, the SST anomaly has a dipole structure: a strong eastern center at 110°W and a weak

TABLE 4. Simultaneous correlation coefficients calculated for the ENSO anomaly mode (defined as the sum of E_1 and E_2) and interannual component, respectively.

Correlation variables	ENSO anomaly mode			Interannual components		
	50°E–120°E	120°E–160°W	160°W–90°W	50°E–120°E	120°E–160°W	160°W–90°W
u_{850} and u_{200}	−.94	−.99	−.96	−.59	−.57	−.79
u_{850} and u_s	.92	.96	.65	.54	.76	.49

western center at 140°E. The convection (OLR) anomaly also exhibits a dipole structure with the eastern center around 160°W and the western center around 125°E. Thus, over the eastern Pacific positive (negative) SST anomalies are located 50° longitude east of enhanced (suppressed) convection, while over the western Pacific the positive (negative) SST anomalies are slightly (10°–20°) east of the enhanced (suppressed) convection. In his study of the relationship between monthly precipitation and SST variation, Weare (1987) found that the SST variations in the central and eastern Pacific link to those of rainfall about 30° westward, but that no significant SST–rainfall correlation is evident west of the date line.

Also evident is the longitudinal variation of the phase relationship between convection and pressure anomalies. In the vicinity of the maritime continent the anomalous surface low (high) pressure nearly coincides with enhanced (suppressed) convection (Figs. 5, 6, and 7c), while in the eastern Pacific surface low (high) pressure anomaly occurs farther to the east (about 60° long.) of the corresponding enhanced (suppressed) convection.

The phase relationship between convection and the boundary-layer zonal wind anomalies changes quite obviously from the warm pool to cold tongue region. Over the warm pool, the enhanced (suppressed) convection is located in the region where surface westerlies and easterlies converge (diverge), while over the central and eastern Pacific, enhanced (suppressed) convection is almost in phase with enhanced surface westerlies (easterlies) (Figs. 6 and 7c). A schematic diagram of the vertical structure of ENSO anomaly mode is summarized in Fig. 8.

5. Impacts of air–sea interaction on the vertical structure of the ENSO anomaly mode

The observations presented in the preceding section indicate that the structural differences of the updraft branch of the ENSO anomaly mode during the cold and warm phases of SO are essentially similar to structural differences of the anomaly mode between the western and central-eastern Pacific. The temporal variation of the structure from cold to warm phase may thus be a direct consequence of the eastward shift of the developing ENSO anomaly mode from the maritime continent–western Pacific to the central-eastern Pacific. Therefore, an essential question needs to be addressed: What causes the longitudinal differences in the vertical structure of the ENSO anomaly mode? In other words, why do spatial phase relationships among the convection, surface zonal wind, surface pressure, and SST undergo substantial changes across the Pacific basin? To answer this question, let us examine the difference in the air–sea interaction processes between the west and east in the Pacific. We will present a conceptual rather than quantitative discussion.

Over the maritime continent and western Pacific where the underlying SST is nearly uniform and higher than 28.5°C, the enhanced (suppressed) convection anomaly centered at 125°E generally overlays a higher (lower) than normal SST region between 110° and 160°E. This positive correlation between the SST and convection anomalies indicates the effect of the variation of SST on the convective variability in the warm pool region. Note, however, that the SST fluctuation is small (only a few tenths of a degree, Fig. 5), yet the OLR fluctuation is relatively pronounced (15–25 W m^{-2}). Besides, the anomalous convection centers are about 15° to the west of the anomalous SST centers and more or less located close to Indonesia. The strong convection variation around 125°E cannot be solely attributed to the SST effect. Under normal conditions the land and sea breeze provide a mechanism for round the clock convection—over land during the day and over offshore oceans during the night (Houze et al. 1981). The moisture convergence induced by the land–ocean thermal contrast constantly causes strong high-frequency (diurnal time scale) convectivity and maintains a semipermanent convective action center in the vicinity of the maritime continent. It appears that the convective intensity in this maximum convection region can be sensitive to the changes in the underlying SST. In another words, the effect of the land–sea thermal contrast may magnify the influence of SST on convection. It may also cause the shift of the convection center toward the maritime continent.

In this high SST region, the moisture content is high and the moist (or effective) static stability (the vertical gradient of moist static energy) is small so that the adiabatic effect associated with the vertical motion is relatively small. Based on the thermodynamic equation describing the gravest baroclinic mode of the free atmosphere, the increase in convective heating induced by boundary-layer moisture convergence is primarily balanced by a local increase in geopotential thickness or a decrease in the low-level pressure field. Thus, the anomalous surface pressure should be out of phase with anomalous convection. This leads to an in-phase relationship between OLR and p_s anomalies (Fig. 8). The zonal momentum balance along the equator requires that the surface zonal wind converges into (diverges from) surface low (high) pressure because the Coriolis force vanishes. It follows that the enhanced (suppressed) convection must be in phase with enhanced surface zonal wind convergence (divergence) (Fig. 8). In short, in the western Pacific warm pool, enhanced convection is slightly to the west of the maximum SST, in phase with negative pressure anomaly and anomalous zonal wind convergence.

In the central-eastern Pacific, on the other hand, SST is lower than 28.0°C except during ENSO events. Since

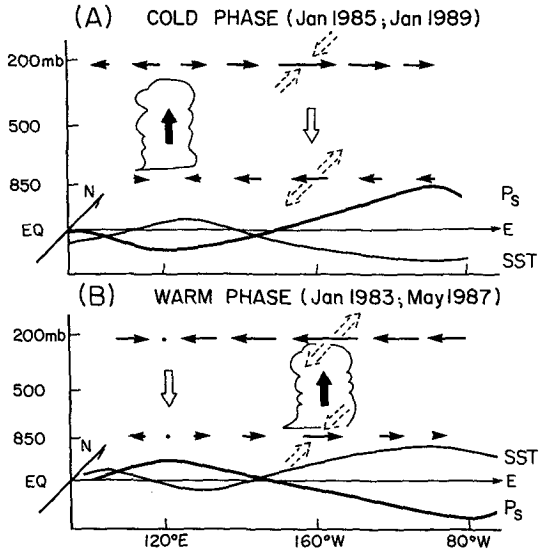

FIG. 8. Schematic diagram of the vertical structure of the ENSO anomaly mode during peak (a) cold and (b) warm phases.

the deep convection usually occurs where SST is higher than 28°C (Graham and Barnett 1987), the movement of active convection is such that it remains in the warm water. It follows that the extent of eastward migration of the active convection as well as the positive convection anomaly is restricted. This may be a partial reason why the eastward-moving enhanced convection centers during warm phases stall in the central Pacific between 170°W and 140°W and do not follow the positive SST anomaly centers farther east. Notice, however, that during the cold phase, SST in the central-eastern Pacific is normally much below the critical temperature 28°C. The nonlinear dependence of convection on SST is no longer a factor that limits the eastward propagation of OLR anomalies. Yet, the suppressed convection (positive OLR anomaly) centers remains stalled in the central Pacific and are located to the west of the negative SST centers with about the same spatial phase difference as that in the warm phase (Fig. 5). This suggests that the spatial phase lag between enhanced (suppressed) convection and positive (negative) SST anomalies cannot be explained simply as a result of dependence of convection upon total SST. It is important to explain why in the central-eastern Pacific the anomalous convection tends to be centered at the region of extreme SST gradients (or extreme surface zonal wind anomaly), rather than extreme SST (or surface pressure) itself.

Over the central and eastern Pacific the SST gradient is much larger than that in the western Pacific. The air–sea interaction is active in the boundary layer where a large SST gradient induces a large pressure gradient via vertical mixing of heat due to buoyant convection forced by surface evaporation. Across the Pacific, high (low) SST is well correlated with low (high) surface pressure, and the positive (negative) zonal SST gradient is correlated with a negative (positive) anomalous pressure gradient (Figs. 5 and 8). Near the equator, Coriolis force vanishes and the large zonal pressure gradient maintains a relatively strong zonal wind ($u_s \sim \partial - p/\partial x$). The boundary-layer convergence is primarily attributed to the meridional wind convergence caused by the meridional variation of Coriolis parameter (beta effect). The beta-induced convergence (divergence) accompanies westerlies (easterlies) (Lindzen and Nigam 1987). Since the boundary-layer moisture convergence plays a crucial role in determining the distribution of anomalous convectivity, the enhanced (suppressed) convection should be in phase with boundary-layer anomalous westerlies (easterlies) or the negative (positive) zonal pressure gradient and positive (negative) zonal SST gradient.

One may question how important is the feedback of the free atmospheric heating to the boundary-layer flow in the eastern Pacific. Since the atmospheric moisture content is relatively low due to the existence of the inversion and due to lower underlying SST, the effective static stability is relatively large. This leads to a dominant balance in the free atmospheric thermodynamics between the convective heating and adiabatic cooling associated with upward motion. As a result, the pressure change at the top of the boundary layer (or the change of geopotential thickness) can be relatively small.

In summary, in the maritime continent and western Pacific the atmospheric motion in both free atmosphere and boundary layer is primarily controlled by the convective heating that is, to some extent, phase locked with the land–sea thermal contrast–induced moisture convergence. In the central Pacific, however, the boundary-layer air–sea interaction plays a major role in determining the vertical structure of the ENSO anomaly mode. The characteristic structure of the ENSO mode across the entire Pacific depicted in Fig. 8 is similar to that shown in Figs. 6 and 7c.

6. Conclusions and discussions

The interannual variabilities of the coupled ocean–atmosphere system along the equatorial Indian and Pacific oceans between 5°N and 5°S are studied for the interval 1979–1989.

The latest two Pacific basinwide warm episodes (1982–83 and 1986–87) exhibits some noticeable common features regardless of their different amplitude and phase. The onset (as well as the peak) phases of 1982–83 and 1986–87 episodes occur in different calendar months that are nearly one half year apart (Fig. 3). This makes it difficult to study composite ENSO mode in a seasonal sequence. Many common features, however, are revealed by multivariate empirical or-

thogonal function (MV-EOF) analysis of the interannual components of the coupled ocean–atmosphere system. By making use of the property of both spatial and intervariable correlation, the MV-EOF effectively filters out noncoherent variations and extracts coherent ENSO signals among a variety of fields of the ocean–atmosphere system. The first two EOFs, which carry two-thirds of the total interannual variance, are defined as ENSO anomaly mode in the present study.

The ENSO anomaly modes in both events exhibit unstable dipole structures: their updraft branches (warm poles) intensify over the western Pacific, while the downdraft branches enhance over the eastern Indian Ocean. The early development of the Pacific warming is evidenced by 1) the strengthening of the cross-equatorial southerly flow over the eastern Pacific and 2) the enhancement of the westerlies and convection over the western Pacific around 160°E (the second EOF mode in Fig. 4).

The aforementioned early development characteristics should not be viewed as precursors for further basinwide warming. They are results of a local warming in the western-central Pacific that does not necessarily lead to a major eastern Pacific warming, as in the case of the "aborted" El Niño in 1980. The western-central Pacific warming in 1990 is probably another example. The conditions under which a weak western-central Pacific warming will further develop to yield a major eastern Pacific warming need to be further investigated. The early warming over the western-central Pacific results from inherent instability of the coupled ocean–atmosphere system. However, the conditions for the realization of the unstable development are not clear. A possible scenario is that the eastward shift of the normal Walker circulation precludes subsequent intensification of the anomaly mode. Yet, what is responsible for the initial eastward shift of the Walker circulation remains unknown in the present analysis. The trigger and forcing resulting from annual or intraseasonal variability have been suggested (Meehl 1987; Lau and Shen 1988). This, along with possible triggers from outside of the equatorial waveguide, should be further explored.

The vertical structure of the *developing* ENSO anomaly modes in the equatorial zonal plane is similar during the two warm episodes. Positive SST anomalies lead enhanced convection by about 25° longitude or one-eighth of the wavelength (Fig. 7b). Murakami (1990) postulated that this phase difference is caused by radiational and turbulent mixing effects associated with low-frequency convection anomaly and favors the eastward propagation of the ENSO mode. This has not been properly explained in the theoretical modeling of the instability of the coupled model. Another noticeable feature is that the convection anomaly is nearly in phase with surface and 850-mb westerly and 200-mb easterly anomalies. This feature is similar to that of the intraseasonal disturbances (Rui and Wang 1990), but differs from that of Gill's solution (Gill 1980) for the atmospheric response to a fixed heat source.

Differences in the vertical structure of the coupled anomaly mode are evident between the warm and cold phases of the Southern Oscillation. In the cold phase, the enhanced convection is slightly west of a positive SST anomaly and in phase with the surface low pressure and anomalous zonal wind convergence (Fig. 6). In the warm phase, on the other hand, the enhanced convection lags positive SST and surface low pressure anomalies by about a quarter wavelength and is nearly in phase with the surface westerly anomaly (Fig. 7c).

It is also found that the structure of the ENSO anomaly mode varies remarkably from the warm pool to cold tongue regardless of the phase of the Southern Oscillation. In the maritime continent–western Pacific region, the enhanced (suppressed) convection tends to be located close to Indonesia and 15° west of positive (negative) SST anomaly and nearly coincides with decreased (increased) surface pressure and anomalous zonal wind convergence (divergence). In the central-eastern Pacific, however, the enhanced (suppressed) convection is nearly in phase with surface westerly (easterly) anomaly, or the positive (negative) zonal SST gradient and negative (positive) zonal pressure gradient. This longitudinal dependence of the vertical structure can be highlighted by Fig. 8.

It is argued that the structural differences of ENSO mode between the warm and cold phases of SO may arise from its eastward migration and the intrinsic longitudinal dependence of the structure of the ENSO anomaly mode. The latter crucially depends on the east–west contrast in the Pacific air–sea interaction processes. In the Indonesia and western Pacific, anomalous convection tends to be phase locked with the effects of the land–sea thermal contrast and sensitively modulated by SST variation. Due to small moist (effective) static stability, the free atmosphere heating controls the variation of surface pressure and corresponding zonal wind anomaly patterns. The resultant vertical structure of the ENSO anomaly mode amounts to that of Gill's model (Gill 1980). In contrast, in the central-eastern Pacific the SST gradient-induced pressure gradient force drives boundary-layer flows whose beta convergence determines the atmospheric heating distribution, whereas the free atmospheric feedback to the boundary-layer flow is weak due to large static stability. The vertical structure of the ENSO anomaly mode is better depicted by the Lindzen and Nigam (1987) model. The structural variation of the ENSO anomaly mode across the Pacific, therefore, is rooted in the zonal inhomogeneity of the mean SST field and different ocean–atmosphere interaction processes.

The RC composites show both an eastward-migrating signal coming from the western Pacific and a westward-migrating signal from the eastern Pacific. The

latter is much stronger than the former. The westward migration in the eastern Pacific was shown to be similar in the evolution of both annual and ENSO signals in a coupled ocean–atmosphere general circulation model (Meehl 1990) and observations (RC; Horel 1982). The 1982–83 and 1986–87 warm events show large SST anomalies originating in the western Pacific and moving east (Gill and Rasmusson 1983; Kousky and Leetmaa 1989). The results derived from the present analysis show a more evident eastward migration of signals in atmospheric circulation anomalies. The eastward evolution of SST, OLR, and wind signals from the Indian to the Pacific Ocean was shown to involve an apparent modulation of the annual cycle (Meehl 1987; Yasunari 1990; Rasmusson et al. 1990). In the coarse-resolution coupled ocean–atmosphere general circulation models, the ENSO events involve only one subset of coupled mechanisms, operating in the eastern Pacific so that the anomalies migrate westward from off the coast of South America (Philander et al. 1989; Meehl 1990). Neither model simulates the western Pacific signals that appear to be important for the latest two warm events. Both the global coupled-model simulations and the present observational analysis indicate that individual ENSO events may display different combinations of various geographically dependent coupling mechanisms, especially with regard to those that seem to work in the eastern Pacific cold tongue and those in the western Pacific warm pool.

In view of the baroclinic structure in the free atmosphere and barotropic structure in the boundary layer of the ENSO anomaly mode, the coupled boundary layer–free atmosphere model developed in Wang (1988) and Wang and Rui (1990) may be used as the simplest dynamic framework to describe ENSO anomaly mode. By adding an SST-induced pressure gradient force in the boundary-layer momentum equation, this model can be viewed as a combination of the Gill (1980)-type and Lindzen–Nigam (1987) models. The essence of the model is the interaction among SST, boundary-layer flow, and free atmospheric heating. Such a model is currently under development.

Because of limited data the present study is confined to the SST and six atmospheric fields. The lack of oceanic mixed-layer data (currents, thermocline depths, etc.) makes it impossible to document detailed features of the oceanic component of the ENSO. The derived results are also subject to the limitations of short data records and the two-dimensional description. Based on an analysis of longer records, Storch et al. (1990) found that eastward movement exists during some cold phases of the Southern Oscillation. We are currently extending the analysis to a longer record and to the global tropics.

Acknowledgments. The author wishes to thank an anonymous referee's relevant comments that led to a much improved manuscript. A part of the discussions in the last section was stimulated by one reviewer's comments. The author is indebted to Prof. T. Murakami for fruitful discussions. Thanks also extend to Mr. C. Wan, Ms. Joanne Huong, and Ms. Diane Henderson for computational, graphical, and technical assistance. This research is supported by EPOCS program of NOAA under Grant No NA-90-RAH-00074.

REFERENCES

Barnett, T. P., 1984a: Interaction of the Monsoon and Pacific trade-wind system at interannual time scales. Part II: The tropical band. *Mon. Wea. Rev.*, **112**, 2380–2387.

——, 1984b: Interaction of the Monsoon and Pacific tradewind system at interannual time scales. Part III: A partial anatomy of the Southern Oscillation. *Mon. Wea. Rev.*, **112**, 2388–2400.

Battisti, D. S., 1988: The dynamics and thermodynamics of a warming event in a coupled tropical atmosphere/ocean model. *J. Atmos. Sci.*, **45**, 2889–2919.

Deser, C., 1990: Meterological characteristics of the El Niño/Southern Oscillation phenomenon. Ph.D. dissertation, University of Washington, 194 pp.

Fu, C., H. F. Diaz, and J. Fletcher, 1986: Characteristics of the response of sea surface temperature in the central Pacific associated with warm episodes of the Southern Oscillation. *Mon. Wea. Rev.*, **114**, 1716–1738.

Gill, A. E., 1980: Some simple solutions for heat induced tropical circulation. *Quart. J. Roy. Meteor. Soc.*, **106**, 447–462.

——, and E. M. Rasmusson, 1983: The 1982–83 climate anomaly in the equatorial Pacific. *Nature*, **306**, 229–234.

Graham, N. E., and T. P. Barnett, 1987: Sea surface temperature, surface wind divergence, and convection over tropical oceans, *Sciences*, **238**, 657–659.

Gutzler, D. S., and D. E. Harrison, 1987: The structure and evolution of seasonal wind anomalies over the near-equatorial eastern Indian and western Pacific oceans. *Mon. Wea. Rev.*, **115**, 169–192.

Harrison, D. E., and D. S. Gutzler, 1986: Variability of monthly-averaged surface and 850 mb winds at tropical Pacific islands. *Mon. Wea. Rev.*, **114**, 285–294.

Hirst, A. C., 1986: Unstable and damped equatorial modes in simple coupled ocean–atmosphere models. *J. Atmos. Sci.*, **43**, 606–630.

Horel, J. D., 1982: The annual cycle in the tropical Pacific atmosphere and ocean. *Mon. Wea. Rev.*, **110**, 1863–1878.

Houze, R. A., S. G. Geotis, F. D. Marks Jr., and A. K. West, 1981: Winter monsoon convection in the vicinity of North Borneo. Part I: Structure and time variation of the cloud and precipitation. *Mon. Wea. Rev.*, **109**, 1595–1614.

Kousky, V. E., and A. Leetmaa, 1989: The 1986–87 Pacific warm episode: Evolution of oceanic and atmospheric anomaly fields. *J. Climate*, **2**, 254–267.

Lau, K.-M., and S. Shen, 1988: On the dynamics of intrasesonal Oscillation and ENSO. *J. Atmos. Sci.*, **45**, 964–979.

Lindzen, R. S., and S. Nigam, 1987: On the role of the surface temperature gradients in forcing low level winds and convergence in the tropics. *J. Atmos. Sci.*, **44**, 2440–2458.

Meehl, G. A., 1987: The annual cycle and interannual variability in the tropical Pacific and Indian ocean region. *Mon. Wea. Rev.*, **115**, 17–50.

——, 1990: Seasonal cycle forcing of El Niño–Southern Oscillation in a global, coupled ocean–atmosphere GCM. *J. Climate*, **3**, 72–98.

Murakami, T., and W. L. Sumathipala, 1988: Relationship between outgoing longwave radiation and sea surface temperature on

interannual time scale. UHMET 88-03, University of Hawaii, 56 pp.

Murakami, T., 1990: Equatorial disturbances, monsoons, and 1982–83 ENSO. *Meteor. Atmos. Phys.* **44,** 85–100.

Neelin, J. D., 1990: The slow sea surface temperature mode and the fast-wave limit: Analytic theory for tropical interannual oscillation and experiments in a hybrid coupled model. *J. Atmos. Sci.,* **48,** 584–606.

Philander, S. G. H., T. Yamagata, and R. C. Pacanowski, 1984: Unstable air–sea interaction in the tropics. *J. Atmos. Sci.,* **41,** 604–613.

——, N.-C. Lau, R. C. Pacanowski, and M. J. Nath, 1989: Two different simulations of Southern Oscillation and El Niño with coupled ocean–atmosphere general circulation models. *Phil. Trans. Roy. Soc.,* 167–178.

Rasmusson, E. M., and T. H. Carpenter, 1982: Variations in tropical sea surface temperature and surface wind fields associated with the Southern Oscillation/El Niño. *Mon. Wea. Rev.,* **110,** 354–384.

——, and J. M. Wallace, 1983: Meteorological aspects of the El Niño/Southern Oscillation. *Science,* **222,** 1195–1202.

——, V. E. Kousky, and M. S. Halpert, 1986: Interannual variability in the equatorial belt: Evolution and relationship to El Niño/Southern Oscillation. *Persistent Meteo-oceanographic Anomalies and Teleconnections.* C. Chagas and G. Puppi, Eds., Pontificiae Academic Scientiarum Scripta Varia, 17–57.

——, X. Wang, and C. F. Ropelewski, 1990: The biennial component of ENSO variability. *J. Mar. Syst.,* **1,** 71–96.

Rui, H., and B. Wang, 1990: Development characteristics and dynamic structure of tropical intraseasonal convection anomalies. *J. Atmos. Sci.,* **47,** 357–379.

Storch, H. V., U. Weese, and J. S. Xu, 1990: Simultaneous analysis of space–time variability: Principal oscillation patterns and principal interaction patterns with applications to the Southern Oscillation. *Z. Meteor.,* **40,** 99–103.

Wang, B., 1988: Dynamics of tropical intraseasonal oscillation: An analysis of moist equatorial Kelvin wave. *J. Atmos. Sci.,* **45,** 2051–2065.

——, and H. Rui, 1990: Dynamics of the coupled moist Kelvin–Rossby wave on an equatorial beta plane. *J. Atmos. Sci.,* **47,** 397–413.

Weare, B. C., 1987: Relationships between monthly precipitation and SST variations in the tropical Pacific region. *Mon. Wea. Rev.,* **115,** 2687–2698.

Wright, P. B., J. M. Wallace, T. P. Mitchell, and C. Deser. 1988: Correlation structure of the El Niño/Southern Oscillation phenomenon. *J. Climate,* **1,** 609–625.

Wyrtki, C., 1975: El Niño—the dynamic response of the equatorial Pacific Ocean to atmospheric forcing. *J. Phys. Oceanogr.,* **5,** 572–584.

Yasunari, T., 1985: Zonally propagating modes of the global east–west circulation associated with the Southern Oscillation. *J. Meteor. Soc. Japan,* **63,** 1013–1029.

——, 1990: Impact of Indian monsoon on the coupled atmosphere/ocean system in the tropical Pacific. *Meteor. Atmos. Phys.,* **44,** 29–41.

Zebiak, S. E., and M. A. Cane, 1987: A model ENSO. *Mon. Wea. Rev.,* **115,** 2262–2278.